

PCCP

Physical Chemistry Chemical Physics

Accepted Manuscript

This article can be cited before page numbers have been issued, to do this please use: J. M. García-Garrido, V. Milner, C. P. Koch and R. Gonzalez-Ferez, *Phys. Chem. Chem. Phys.*, 2026, DOI: 10.1039/D5CP02931G.



This is an Accepted Manuscript, which has been through the Royal Society of Chemistry peer review process and has been accepted for publication.

Accepted Manuscripts are published online shortly after acceptance, before technical editing, formatting and proof reading. Using this free service, authors can make their results available to the community, in citable form, before we publish the edited article. We will replace this Accepted Manuscript with the edited and formatted Advance Article as soon as it is available.

You can find more information about Accepted Manuscripts in the [Information for Authors](#).

Please note that technical editing may introduce minor changes to the text and/or graphics, which may alter content. The journal's standard [Terms & Conditions](#) and the [Ethical guidelines](#) still apply. In no event shall the Royal Society of Chemistry be held responsible for any errors or omissions in this Accepted Manuscript or any consequences arising from the use of any information it contains.

Cite this: DOI: 00.0000/xxxxxxxxxx

Rotational excitation of molecules in the regime of strong ro-vibrational coupling: Comparison between an optical centrifuge and a transform-limited pulse

J.M. García-Garrido,^a V. Milner,^b C.P. Koch^c and R. González-Férez^{a,d}Received Date
Accepted Date

DOI: 00.0000/xxxxxxxxxx

We investigate theoretically the ability of an optical centrifuge – a laser pulse whose linear polarization is rotating at an accelerated rate, to control molecular rotation in the regime when the rigid-rotor approximation breaks down due to coupling between the vibrational and rotational degrees of freedom. Our analysis demonstrates that the centrifuge field enables controlled excitation of high rotational states while maintaining relatively low spread along the vibrational coordinate. We contrast this to the rotational excitation by a linearly polarized Gaussian pulse of equal spectral width and pulse energy which, although comparable to the centrifuge-induced rotation, is unavoidably accompanied by a substantial broadening of the vibrational wavepacket.

1 Introduction

Laser pulses have long been used for controlling the rotation of molecules^{1–4}. Among multiple approaches to rotational control, the method of an optical centrifuge proved to be most successful in spinning molecules to extremely high rotational states, known as molecular super-rotors^{5,6}. The centrifuge is a linearly polarized laser pulse, whose polarization vector rotates with a constant angular acceleration. An interaction of the laser-induced dipole moment with the applied laser field results in a torque, which forces the molecule to follow the accelerated rotation of the field polarization.

On the experimental side, optical centrifuges have been used in numerous studies of molecular structure and molecular dynamics (for recent reviews, see Refs. 7,8). In these investigations, it has been assumed that the centrifuge drives the molecule up the rotational ladder of states, without explicitly driving Raman transitions up the vibrational manifold. This approximation is well justified in the case of relatively light molecular species with strong molecular bonds and correspondingly high energies of Raman-active vibrational modes (i.e. $> 1000\text{ cm}^{-1}$), which fall outside the available energy bandwidth of amplified femtosecond laser pulses ($\sim 500\text{ cm}^{-1}$).

In the case of heavier molecules, or those with softer molecular bonds, ro-vibrational coupling may significantly change the dynamics of a super-rotor. Previous theoretical studies have explored this scenario in the context of the centrifuge-induced dissociation^{9–11}, as well as the dissociation induced by a short laser pulse¹². Interestingly, the reverse process of creating a molecular bond can also be facilitated by the ro-vibrational coupling¹³. On the experimental side, evidence of the ro-vibrational energy exchange in the field-free dynamics of molecules in extreme rotational states has been recently reported¹⁴.

Dissociation is an extreme example of coupled ro-vibrational dynamics. In view of coherent control of ro-vibrational dynamics, it is also interesting to understand the spread of population across the vibrational manifold below the dissociation limit. One of the open questions is whether the optical centrifuge can provide an experimental tool to make the molecule climb the vibrational ladder in a controlled way (much like it does with the rotational ladder climbing). Alternatively, one may ask whether high rotational excitation of molecules with low vibrational energies can be executed with the optical centrifuge in such a way as to keep their vibrational state intact, thus protecting them from the potential dissociation. Heavier molecules may be susceptible to the vibrational excitation by the centrifuge field, leading to ro-vibrational coupling, which may significantly change the dynamics of a super-rotor.

Our aim here is to analyze theoretically the degree of the vibrational excitation, comparing the effect of the centrifuge with that of a simple Gaussian pulse. To this end, we have carried out a full quantum mechanical analysis of the ro-vibrational dynamics of a diatomic molecule in a non-resonant laser field. We compare a

^a Departamento de Física Atómica, Molecular y Nuclear, Universidad de Granada, 18071 Granada, Spain.

^b Department of Physics and Astronomy, The University of British Columbia, Vancouver, Canada.

^c Freie Universität Berlin, Dahlem Center for Complex Quantum Systems and Fachbereich Physik, Germany.

^d Instituto Carlos I de Física Teórica y Computacional, Universidad de Granada, 18071 Granada, Spain.



pulse whose time envelope mimics one of the polarization axis of an optical centrifuge¹⁵ with a Gaussian pulse with the same spectral bandwidth and carrying the same energy as the centrifuge pulse. We have chosen Rb₂ as an example of a heavy diatomic molecule that can be prepared and studied in a trapped ultracold gas^{16–19}.

This article is organized as follows. In section 2 we describe the system Hamiltonian including the interaction with the optical centrifuge and another non-resonant laser pulse. Section 3 is devoted to explore the field-dressed dynamics of the rovibrational ground state and of several excited states as well as of a thermal sample. Conclusions and outlook are presented in section 4.

2 System description and numerical method

We consider a diatomic molecule in the $a^3\Sigma^+$ electronic state exposed to a non-resonant laser pulse linearly polarized along the Z-axis of the laboratory-fixed frame (LFF). Within the Born-Oppenheimer approximation, the nuclear Hamiltonian is given by

$$H(t) = T_R + \frac{\mathbf{N}^2}{2\mu R^2} + V(R) + H_I(t), \quad (1)$$

where the first and second terms stand for the vibrational and rotational kinetic energies, respectively, \mathbf{N} is the rotational angular momentum, μ the reduced mass of the molecule, R the internuclear distance, and $V(R)$ the electronic potential energy curve. For a non-resonant laser field, the polarizability interaction reads

$$H_I(t) = -\frac{I(t)}{2c\epsilon_0} (\Delta\alpha(R)\cos^2\theta + \alpha_{\perp}(R)), \quad (2)$$

where $I(t)$ is the intensity of the laser field, c the speed of light in vacuum, ϵ_0 the electric permittivity of vacuum, and θ is the Euler angle formed between the internuclear and laser polarization axes. The polarizability anisotropy is $\Delta\alpha(R) = \alpha_{\parallel}(R) - \alpha_{\perp}(R)$, with $\alpha_{\parallel}(R)$ and $\alpha_{\perp}(R)$ being the parallel and perpendicular components of the polarizability in the molecular-fixed frame (MFF).

The time-dependent Schrödinger equation associated with the Hamiltonian (1) is solved by a grid representation of the wave function, i.e., the Fourier and discrete variable representations for the radial and angular coordinates, respectively^{20–22}, and the time evolution is calculated using the Chebyshev propagator²³. The field-dressed dynamics is analyzed in terms of the field-free rovibrational eigenstates of the Hamiltonian (1) (obtained by setting $t = 0$), $\Phi_{v,N,M_N}(\mathbf{R}) = \phi_{v,N}(R)Y_{N,M_N}(\theta, \varphi)$, where $\phi_{v,N}(R)$ and $Y_{N,M_N}(\theta, \varphi)$ are the vibrational and rotational parts, respectively, with $Y_{N,M_N}(\theta, \varphi)$ being the spherical harmonics, and (v, N, M) the vibrational, rotational, and magnetic quantum numbers. For the sake of simplicity, we refer to the eigenstate $\Phi_{v,N,M_N}(\mathbf{R})$ by its quantum numbers (v, N, M) . For a given initial state $\Psi(\mathbf{R}, t = 0) = \Phi_{v_0, N_0, M_{N_0}}(\mathbf{R})$, the time-dependent wave function can be expressed as

$$\Psi(\mathbf{R}, t) = \sum_{v,N} C_{v_0, N_0, M_{N_0}}(v, N, t) \Phi_{v, N, M_N}(\mathbf{R}, t), \quad (3)$$

where the sum runs over all vibrational bands and rotational excitations up to a maximal value, which is chosen to ensure

converged results. In this expansion (3), we have used that M_{N_0} is a good quantum number due to the azimuthal symmetry. The coefficients $C_{v_0, N_0, M_{N_0}}(v, N, t)$ depend on time during the pulse duration. Afterwards, the Hamiltonian (1) becomes time-independent, and these coefficients acquire constant absolute values but varying phases.

We consider two different laser fields, both linearly polarized along the LFF Z-axis. The first one is a “two-dimensional” centrifuge pulse (CP), which mimics the experimental pulses used in²⁴. While the two-dimensional model greatly simplifies our analysis, we expect its result to apply to conventional three-dimensional centrifuge fields¹⁵, because our focus is on the effects which do not depend on the directionality of molecular rotation. The intensity of this pulse is given by

$$I_C(t) = \begin{cases} I_C^0 \sin^2\left(\frac{\pi t}{2t_0}\right) g(t; \beta), & 0 \leq t \leq t_0, \\ I_C^0 g(t; \beta), & t_0 < t \leq t_C - t_0, \\ I_C^0 \sin^2\left(\frac{\pi(t_C - t)}{2t_0}\right) g(t; \beta), & t_C - t_0 < t \leq t_C, \end{cases} \quad (4)$$

where I_C^0 is the peak intensity, t_0 the turning on and off time, and t_C the duration of this pulse. The function $g(t; \beta) = \sin^2(\beta t^2)$ simulates the oscillatory behavior of an experimental optical centrifuge pulse, with the parameter β being the analogue of the acceleration of the polarization axis rotation. Here, the CP parameters are fixed to $\beta = 0.3 \text{ ps}^{-2}$, $t_0 = 3 \text{ ps}$ and $t_C = 15 \text{ ps}$.

The second pulse is a non-modulated Gaussian pulse (GP) with the same spectral bandwidth as the CP, and intensity

$$I_G(t) = I_G^0 \exp\left(-\frac{(t - t_g)^2}{\sigma^2}\right), \quad (5)$$

where I_G^0 is the peak intensity and $2\sigma\sqrt{\log 2}$ is the full width at half maximum (FWHM). This GP possesses the same spectral bandwidth as the considered CP if σ is taken to be $\sigma = 0.142 \text{ ps}$. In addition, we impose that both pulses carry the same energy, which happens when their peak intensities are related to one another as $I_G^0 = 24.05 I_C^0$. The GP is centered at $t_g = 0.671 \text{ ps}$, twice the value of the FWHM of the GP, so that the intensity at $t = 0 \text{ ps}$ is $\sim I_G^0 \cdot 10^{-10} \text{ W/cm}^2$. The duration of this pulse is $t_G = 2t_g \text{ ps}$, i.e., four times the GP FWHM. By fixing this value of t_G , we have ensured that the effects due to very small, but non-zero, laser fields at the beginning and end of the time-evolution are negligible.

3 Field-dressed rovibrational dynamics

We consider a Rb₂ molecule for which the lowest triplet electronic state $a^3\Sigma_u^+$ accommodates approximately 41 vibrational states with no rotational excitation, i.e., $N = 0$. Note that due to the molecular symmetries, the $a^3\Sigma_u^+$ potential only accommodates rotational states of even parity. The number of bound rotational excitations decreases as the vibrational quantum number v increases. For instance, the maximal values of the rotational quantum numbers are $N = 152, 5$ and 0 for the vibrational bands $v = 0, 39$ and 40 , respectively. For the lowest vibrational band of Rb₂ in the $a^3\Sigma_u^+$ electronic state, the rotational constant is 0.0104 cm^{-1} , whereas the vibrational splitting is 12.8 cm^{-1} .

The interaction with the laser field, for moderate to strong in-



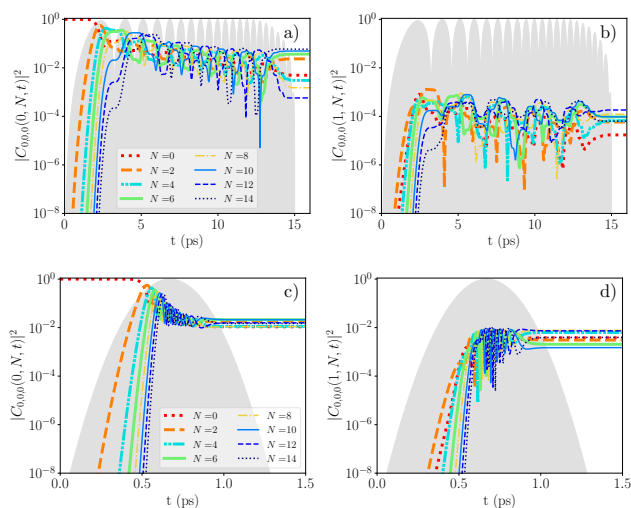


Fig. 1 For the initial state $(0,0,0)$, time evolution of the weights of the field-free states $|C_{0,0,0}(v, N, t)|^2$ with rotational quantum number $N \leq 14$ and vibrational quantum numbers a) and c) $v = 0$; and b) and d) $v = 1$. The peak intensities are $I_G^0 = 10^{12}$ W/cm 2 and $I_C^0 = 4.158 \cdot 10^{10}$ W/cm 2 . The shaded areas represent the time profiles of the pulses.

tensities, is expected to lead to a significant hybridization of the rotational motion, followed by an impulsive alignment because their durations are significantly shorter than the Rb $_2$ rotational period of $\tau_B = 1.6$ ns. However, the field-induced dressed dynamics for the CP and GP should be different due to the very distinct time scales and ways in which the pulses transfer the same energy to the molecule.

3.1 Dynamics of the rovibrational ground state

We assume that Rb $_2$ is initially in its rovibrational ground state $(0,0,0)$ and analyze the dressed dynamics by the time-evolution of the projections of the wavepacket into the field-free basis, i. e., $|C_{0,0,0}(v, N, t)|^2$, presented in Figure 1. We only plot the coefficients of the field-free states with $v = 0, 1$ and $N \leq 14$. For the G and C pulses, the peak intensities are fixed to $I_G^0 = 10^{12}$ W/cm 2 and $I_C^0 = 4.158 \cdot 10^{10}$ W/cm 2 , respectively. Due to the selection rules $\Delta N = \pm 2$ of the field interaction, $(0,2,0)$ is the first state contributing to the field-dressed wavepacket, and immediately afterwards, higher rotational excitations are also populated. The weights $|C_{0,0,0}(0, N, t)|^2$ initially increase up to a maximum, keeping an oscillatory behavior till the end of the pulse when they reach a final constant value. For the CP, the oscillatory behavior of $|C_{0,0,0}(0, N, t)|^2$ is a bit more irregular due to the consecutive maxima of $I_C(t)$. The low values of the weights plotted in Figure 1 indicate that many rotational excitations contribute to the wave function.

An interesting phenomenon is that both pulses provoke that states within neighboring vibrational bands get populated. The comparison between panels (b) and (d) of Figure 1 shows that their contribution is more important for the GP-dressed wavepacket, but even so, they cannot be neglected for a proper description of the CP-induced dynamics. These non-zero weights of states with $v > 0$ proves a strong ro-vibrational coupling be-

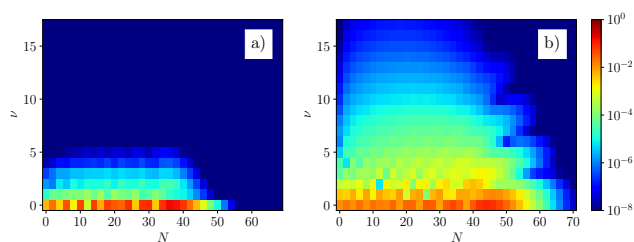


Fig. 2 For the initial state $(0,0,0)$, final weights of the field-free rovibrational states $|C_{v,N}^0(t_f)|^2$ after the a) centrifuge and b) Gaussian pulses with peak intensities $I_G^0 = 10^{12}$ W/cm 2 and $I_C^0 = 4.158 \cdot 10^{10}$ W/cm 2 , respectively.

tween the vibrational and rotational degrees of freedom, induced by the interaction with the non-resonant laser field, and the breakdown of the rigid-rotor approximation. The contribution of states from higher vibrational bands is also important at the end of the pulses, as shown by the weights of the field-free eigenstates plotted in Figure 2 (a) and Figure 2 (b) for the G and C pulses, respectively. These final weights illustrate the differences between the dynamics induced by these two fields. The distribution of population is wider in the vibrational and rotational quantum numbers for the GP-induced dynamics. For instance, the neighboring vibrational bands $v = 1$ and $v = 2$ have larger cumulative weights, defined in Equation 8, $\mathcal{V}_{0,0,0}(1, t_f) = 0.160$ and $\mathcal{V}_{0,0,0}(2, t_f) = 0.033$ due to the GP. In contrast, the vibrational distribution induced by the CP pulse is very narrow, with rather low cumulative weights, $\mathcal{V}_{0,0,0}(1, t_f) = 0.0018$ and $\mathcal{V}_{0,0,0}(2, t_f) = 0.0003$, which is due to its weaker peak intensity, and its gradual transfer of energy to the molecule. Indeed, the centrifuge time envelope enables a better control over the vibrational excitations that are not significantly increased after the first intensity maximum.

An experimental optical centrifuge creates molecular samples in super-rotor states, i. e., in very high rotational excitations¹⁵. We analyze this property by the final cumulative weights in a certain rotational quantum number, independently of their vibrational band, $\mathcal{N}_{0,0,0}(N, t_f)$ defined in Equation 9. $\mathcal{N}_{0,0,0}(N, t_f)$ is plotted as a function of N in Figure 3 (a) and (b) for the G and C pulses, respectively. In addition, Figure 3 shows the final weights in a certain rotational excitation obtained within the rigid-rotor description, see Appendix A. The GP-dressed dynamics involves many rotational excitations, $\mathcal{N}_{0,0,0}(N, t_f)$ shows small-amplitude oscillations as N increases and reaches a global maximum at $N = 44$, decreasing afterwards. The rigid-rotor approximation does not reproduce the rovibrational results due to the large contribution from neighboring vibrational bands. For the CP-induced dynamics, $\mathcal{N}_{0,0,0}(N, t_f)$ also oscillates with N with larger amplitudes, and reaches its global maximum at $N = 36$, approaching zero for higher values of N . For the CP case, rigid-rotor description provides a good approximation because the contributions from higher vibrational bands is rather small at the weak peak intensity of the CP. The mean rotational excitations, defined in Equation 10, are $\langle \mathcal{N}_{0,0,0} \rangle = 32.2$ and 27.6 for the GP and CP, respectively. These mean values indicate that



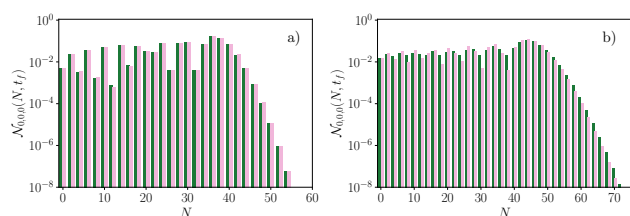


Fig. 3 For the initial state $(0,0,0)$, final population distribution (dark green) according to rotational quantum number N defined in Equation 9 after the a) centrifuge and b) Gaussian pulses with peak intensities $I_C^0 = 4.158 \cdot 10^{10} \text{ W/cm}^2$ and $I_G^0 = 10^{12} \text{ W/cm}^2$, respectively. For the rigid-rotor approximation (light pink), we present the weights of each rotational state with the lowest vibrational band $v = 0$.

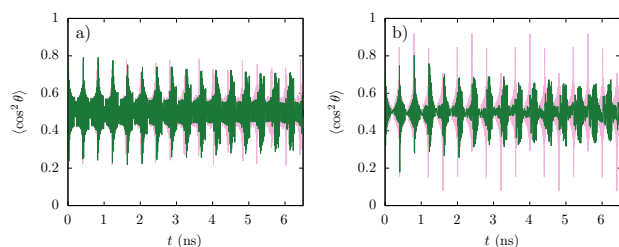


Fig. 4 For the initial state $(0,0,0)$, time evolution of the alignment (dark-green thin line) induced by the a) centrifuge and b) Gaussian pulses with peak intensities $I_G^0 = 10^{12} \text{ W/cm}^2$ and $I_C^0 = 4.158 \cdot 10^{10} \text{ W/cm}^2$, respectively. The alignment computed within the rigid-rotor (light-pink thick line) approximation is also plotted.

the way the energy is transferred by the GP pulse to the ground state give rise to higher rotational excitations than in the CP dynamics.

Non-resonant light is normally used to produce samples of molecules aligned along the laser-polarization axis. The time-evolution of the alignment $\langle \cos^2 \theta \rangle \equiv \langle \Psi(\mathbf{R}, t) | \cos^2 \theta | \Psi(\mathbf{R}, t) \rangle$ induced by these pulses is presented in Figure 4. For comparison, the results obtained within the rigid-rotor approximation are also plotted in this figure. Both pulses provoke an impulsive alignment to the molecule due to their short duration compared to molecular rotational period, with $\langle \cos^2 \theta \rangle$ reaching extreme values at the rotational revivals $k\tau_B/4$, with k being an integer. For the GP-induced alignment, there are large deviations between the rigid-rotor and rovibrational descriptions, due to the important role played by higher vibrational bands on the dressed dynamics. For instance, the alignment obtained with the full rovibrational description possesses smaller maximal values, which are reduced and shifted with respect to the revivals $k\tau_B/4$ as time increases. For the CP-induced alignment, the agreement with the rigid-rotor description is good during (approximately) the first rotational period. Indeed, the narrow vibrational broadening induced by this pulse provokes that the differences between these results and a small reduction of the maximal alignment appear only at later times.

We conclude this section by analyzing the dynamics induced to the initial state $(0,0,0)$ by a CP with a stronger intensity, $I_C^0 = 1.8 \cdot 10^{11} \text{ W/cm}^2$, the weights $|C_{0,0,0}(v, N, t)|^2$ are plotted in Figure 5 at different times. Due to the stronger peak intensity,

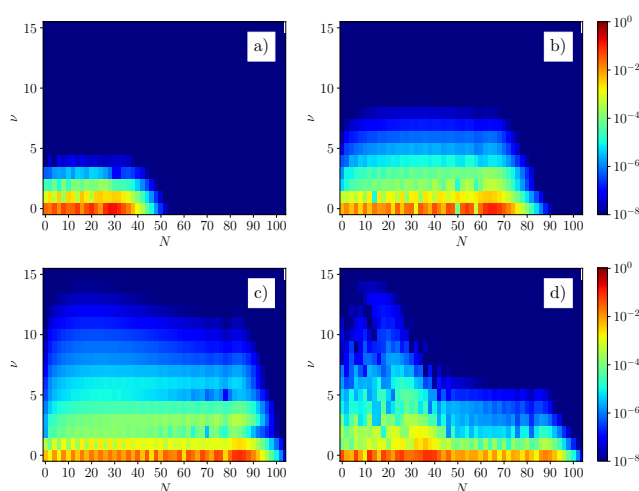


Fig. 5 For the initial state $(0,0,0)$ in a CP, weights $|C_{0,0,0}(v, N, t)|^2$ of the field-free rotational and vibrational states into the field-dressed wavepacket at times a) $t = 2.29 \text{ ps}$ (first maximum of $I_C(t)$); b) $t = 6.86 \text{ ps}$ (fifth maximum); c) $t = 10.97 \text{ ps}$ (twelfth maximum); and d) at the end of the pulse ($t = 15 \text{ ps}$), with peak intensity $I_C^0 = 1.8 \cdot 10^{11} \text{ W/cm}^2$.

already at the first maximum, a significant population is transferred to the vibrational band $v = 1$. By further increasing the time, the distribution of population becomes significantly wider in N , but not in v . At the end of the pulse, there are several vibrational bands with significant contributions $\mathcal{V}_{0,0,0}(1, t = t_f) = 0.028$ and $\mathcal{V}_{0,0,0}(2, t = t_f) = 0.011$. However, despite these moderate vibrational weights, the CP pulse efficiently transfers population to higher rotational excitations reaching the mean value $\langle \mathcal{N}_{v_0, N_0, M_{N_0}} \rangle = 32.8$.

3.2 Dynamics of rovibrational excited states

In this section, we analyze the impact of these two pulses on excited vibrational states taking as prototype example the initial state $(25,0,0)$. Figs. 6 and 7 present the weights $|C_{25,0,0}(v, N, t)|^2$ as a function of v and N at different time steps of the GP- and CP-dressed dynamics, respectively. The peak intensities are fixed to $I_G^0 = 10^{12} \text{ W/cm}^2$ and $I_C^0 = 4.158 \cdot 10^{10} \text{ W/cm}^2$.

At the beginning of the pulses, the population distribution is similar, as illustrated in panels a) of Figs. 6 and 7 for $t = 0.553 \text{ ps}$ and 2.29 ps , respectively. Initially, the rotational excitations within $v_0 = 25$ show the largest contribution to the wavepackets, but those within the neighboring vibrational bands $v_0 \pm 1, 2$ also possess significant weights. As time increases, the differences between the field-dressed dynamics become more evident and are due to the distinct ways that the pulses transfer energy to the molecule. The short duration and high intensity of the GP provoke that significantly more rovibrational states are involved in the dynamics, with a large amount of population transferred to other vibrational bands. This population distribution to neighboring vibrational bands follows a diagonal path due to that the dominant matrix elements between different bands are $\langle v, N, M_N | \Delta \alpha(R) \cos^2 \theta | v \pm 1, N \pm 2, M_N \rangle$, see Figure 12. For the CP wavepacket, more rotational excitations get populated at these later time steps, whereas the total weights of states in differ-



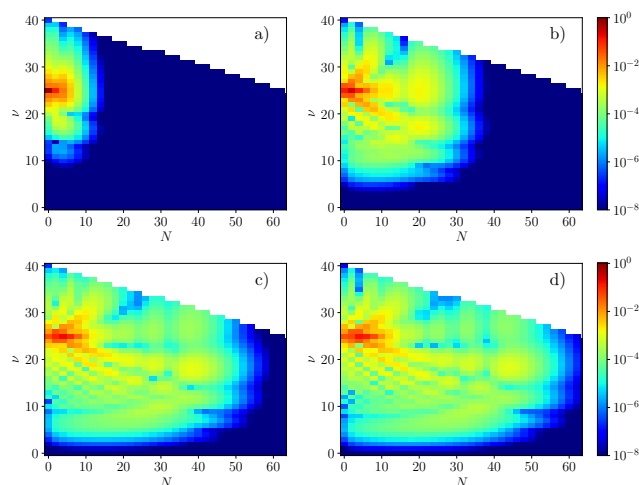


Fig. 6 For the initial state $(25,0,0)$ in a GP, weights $|C_{25,0,0}(v, N, t)|^2$ of the field-free rotational and vibrational states into the field-dressed wavepacket a) at the FWHM $t = 553$ fs; b) at the maximum of the GP $t = t_g = 672$ fs; c) at the FWHM $t = 790$ fs; d) and at the end of the GP. The peak intensity is $I_G^0 = 10^{12}$ W/cm².

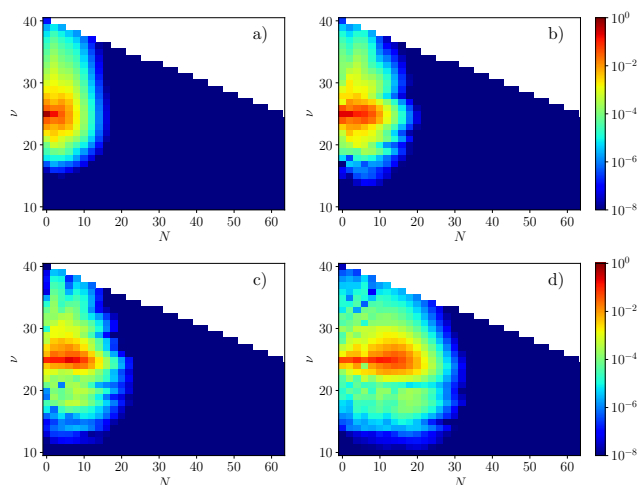


Fig. 7 For the initial state $(25,0,0)$ in a CP, weights $|C_{25,0,0}(v, N, t)|^2$ of the field-free rotational and vibrational states into the field-dressed wavepacket at a) first maximum $t = 2.29$ ps; b) fifth maximum $t = 6.86$ ps; c) twelfth maximum $t = 10.97$ ps; and d) at the end of the pulse $t = 15$ ps. Peak intensity is $I_C^0 = 4.158 \cdot 10^{10}$ W/cm².

ent vibrational bands does not change significantly after the first intensity maximum, being the main contributions from $v_0 \pm 1, 2$ and 3. This controlled spread over vibrational excitations reflects the gradual transfer of energy from the centrifuge field to the molecule. Hence, in this strong coupling regime, the CP pulse is more efficient in creating super-rotor wavepackets formed by high rotational excitations while simultaneously keeping a narrow distribution of vibrational bands.

Compared to the ground state, the impact on this excited state of these laser fields is weaker. This is due to the largest spatial extension of the vibrational wave function as v increases, and the highest probability density being located close to the outermost classical turning point of the electronic potential curve. As a consequence, the overlaps of the corresponding wave functions with the R -dependent polarizabilities are smaller, reducing the impact of the laser field. In contrast to the ground-state, the CP is more efficient climbing the rotational ladder, and at the end of the pulses, the mean values of the rotational excitations are $\langle \mathcal{N}_{25,0,0} \rangle = 10.35$, and 7.90, for the C and G pulses, respectively. For the GP-dressed dynamics, the wider distribution of the final weights in the vibrational and rotational quantum numbers reduces the contributions of highly excited rotational states, and, as a consequence, the mean value $\langle \mathcal{N}_{25,0,0} \rangle$ becomes smaller.

Analogous results are obtained for other vibrational excited state $(v_0, 0, 0)$, as illustrated in Figure 8 with the final distribution of population in the rovibrational spectrum for $v_0 = 5, 10, 35$ and 39, and peak intensities $I_G^0 = 10^{12}$ W/cm² and $I_C^0 = 4.158 \cdot 10^{10}$ W/cm². The dressed dynamics of these states shows similar features as those discussed for $(25,0,0)$ above. For both pulses, we observe that as the vibrational excitation increases, the impact of the laser field is reduced. The stronger impact induced by the GP pulse, gives rise to higher hybridization of the rotational and vibrational motions illustrated by wider distributions among the field-free states. Most important, the CP-induced vibrational

spreading is very narrow for all analyzed cases.

We explore the creation of molecular samples in highly excited rotational states by the final mean value of the rotational excitation $\langle \mathcal{N}_{v_0,0,0} \rangle$ Equation 10, which is presented in Figure 9 as a function of the vibrational excitation v_0 and for several peak intensities of both pulses. As indicated above, the impact of the laser field decreases as v_0 increases, which is manifested on the decreasing trend of $\langle \mathcal{N}_{v_0,0,0} \rangle$. For the lowest peak intensities, $\langle \mathcal{N}_{v_0,0,0} \rangle$ reaches similar values for both pulses. In contrast, for the strongest intensities, the rotational ladder is climbed more (less) efficiently by applying a CP than a GP for the rotational ground states in the vibrational bands with $v_0 \gtrsim 14$ ($v_0 \lesssim 14$). This is due to the broader vibrational distribution induced by the GP for these initial excited states, which reduces the weight of higher rotational excitations, and, therefore, the value of $\langle \mathcal{N}_{v_0,0,0} \rangle$. For the vibrational bands close to the dissociation threshold, $\langle \mathcal{N}_{v_0,0,0} \rangle$ reaches rather low values due to the small amount of rotational excitations bounded in those bands and a weaker field impact.

An important feature of the dressed dynamics is the partial dissociation of the molecule as scattering states also contribute to the final wave function²⁵. This occurs for $(25,0,0)$ in Figure 7 (a), and for $v_0 = 5, 10, 35$ and 39 under the CP in Figure 8. For all these states, we encounter that the upper most rotational excitation bounded within a certain vibrational band is populated. This field-induced dissociation at the end of the pulse is quantified $P_{v_0,0,0}^D$, defined in Equation 11, which is plotted in Figure 10 (a) and (b) as a function of v_0 and for several peak intensities of the G and C pulses, respectively. This field-induced dissociation strongly depends on the initial state, pulse shape and peak intensity. For the GP, $P_{v_0,0,0}^D$ shows a smooth behavior as a function of the vibrational band of the initial state v_0 . $P_{v_0,0,0}^D$ initially increases as v_0 increases, reaching a maximum, and decreasing for highly excited vibrational bands. As the peak intensity increases, a largest amount of population is transferred to the con-



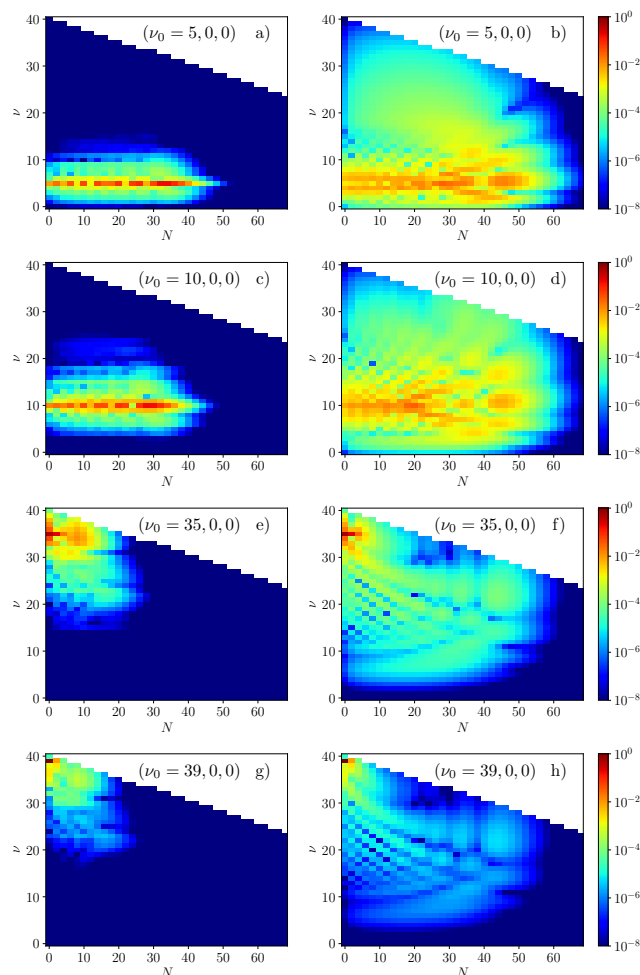


Fig. 8 For the initial states $(\nu_0, 0, 0)$, weights $|C_{\nu_0,0,0}(v, N, t)|^2$ of the field-free rotational and vibrational states into the field-dressed wavepacket at the end of the centrifuge (left column) and Gaussian (right column) pulses with peak intensity $I_G^0 = 10^{12}$ W/cm² and $I_C^0 = 4.158 \cdot 10^{10}$ W/cm², respectively.

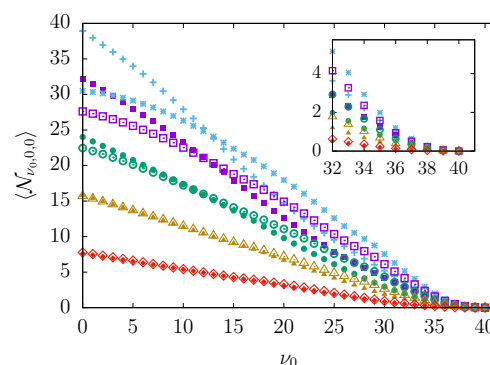


Fig. 9 The accumulative rotational weights at the end of a Gaussian and centrifuge pulse as a function of the vibrational quantum number of the initial states $(\nu_0, 0, 0)$. The inset shows these accumulative rotational weights for initial states close to the dissociation threshold with $\nu_0 \geq 32$. The peak intensities are fixed so that both pulses carry the same energy, and are $I_C^0 = 50.00$ GW/cm² (blue crosses), $I_C^0 = 41.58$ GW/cm² (purple squares), $I_C^0 = 31.18$ GW/cm² (green circles), $I_C^0 = 20.79$ GW/cm² (yellow triangles) and $I_C^0 = 10.39$ GW/cm² (red diamonds), for the centrifuge pulse; and $I_G^0 = 1.203$ TW/cm² (blue stars), $I_G^0 = 1.00$ TW/cm² (purple filled squares), $I_G^0 = 0.75$ TW/cm² (green filled circles), $I_G^0 = 0.50$ TW/cm² (yellow filled triangles) and $I_G^0 = 0.25$ TW/cm² (red filled diamonds) for the Gaussian pulse.

tinuum, and, in addition, the maximum is shifted to lower values of ν_0 , being at $\nu_0 = 36$ and $\nu_0 = 22$ for $I_G^0 = 2.5 \cdot 10^{11}$ W/cm² and $1.203 \cdot 10^{12}$ W/cm², respectively. For the CP, the dependence of $P_{\nu_0,0,0}^D$ on ν_0 changes as I_C^0 increases, transforms from having only one maximum to two, being the global one located at $\nu_0 = 36$ for all considered peak intensities I_G^0 .

The narrower vibrational spreading induced by the CP pulse favors the reduction of the dissociation for most initial states. Indeed, the stronger vibrational impact of the GP is reflected in a higher value of $P_{\nu_0,0,0}^D$ for most of the analyzed states, except for the highly excited vibrational ones lying close to the dissociation limit. For instance, for $\nu_0 = 36$, $P_{\nu_0,0,0}^D = 0.06$ and 0.08 for a GP with $I_G^0 = 10^{12}$ W/cm² and a CP with $I_C^0 = 4.158 \cdot 10^{10}$ W/cm², respectively. For the GP, the ladder-like distribution of population implies that lower-lying vibrational bands are populated, and these bands accommodate more rotational excitations, being, therefore, harder the dissociation. In contrast, at the end of CP, mainly neighboring vibrational bands to $\nu_0 = 36$ are populated, being easier to reach their maximal rotational excitation and facilitating the molecular dissociation.

3.3 Thermal distribution

The results discussed in the previous sections assume either a rotational temperature of 0 K, i.e., the $(0,0,0)$ state, or vibrational excitations but no rotational excitation $N_0 = 0$. Molecular samples in a single rovibrational state are experimentally feasible in the ultracold regime^{26,27}. However, molecular beam experiments are characterized by a certain rotational temperature, being extremely challenging to create molecular samples in a single state^{28–30}. Here, we consider thermal samples of Rb₂ with rotational temperatures that are experimentally feasi-



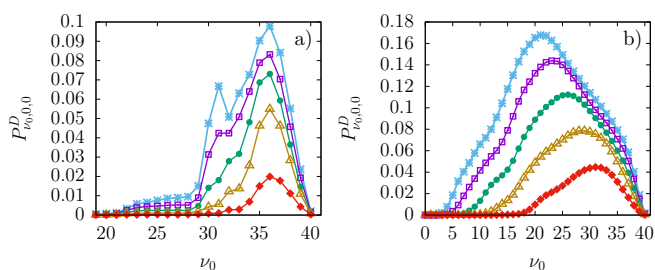


Fig. 10 For the initial states $(v_0, 0, 0)$, population transferred to the continuum Equation 11 at the end of the a) centrifuge and b) Gaussian pulses for several peak intensities: for the centrifuge, $I_C^0 = 50.00 \text{ GW/cm}^2$ (blue stars), $I_C^0 = 41.58 \text{ GW/cm}^2$ (purple squares), $I_C^0 = 31.18 \text{ GW/cm}^2$ (green filled circles), $I_C^0 = 20.79 \text{ GW/cm}^2$ (yellow triangles) and $I_C^0 = 10.39 \text{ GW/cm}^2$ (red filled diamonds), and for the Gaussian, $I_G^0 = 1.203 \text{ TW/cm}^2$ (blue stars), $I_G^0 = 1.00 \text{ TW/cm}^2$ (purple squares), $I_G^0 = 0.75 \text{ TW/cm}^2$ (green filled circles), $I_G^0 = 0.50 \text{ TW/cm}^2$ (yellow triangles) and $I_G^0 = 0.25 \text{ TW/cm}^2$ (red filled diamonds). These intensities have been taken so that both pulses carry the same energy, see section 2.

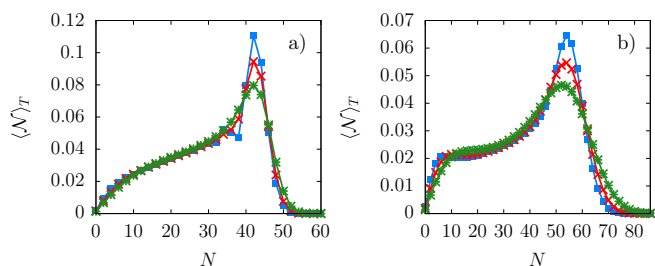


Fig. 11 For thermal samples of Rb_2 at rotational temperatures $T = 0.5 \text{ K}$ (blue squares), $T = 1.0 \text{ K}$ (red crosses) and $T = 2.0 \text{ K}$ (green stars), post-pulse distribution of the population among the rotational states Equation 10 for a) a Centrifuge pulse with $I_C^0 = 5.0 \cdot 10^{10} \text{ W/cm}^2$, and b) a Gaussian pulse with peak intensity $I_G^0 = 1.203 \cdot 10^{12} \text{ W/cm}^2$.

ble $T \leq 2.0 \text{ K}$. In our description, the thermal sample is restricted to states within the lowest vibrational band, i.e., with quantum numbers $(0, N, M_N)$ with $N \leq 24$ and $N \leq M_N \leq N$. Note that for $T = 2 \text{ K}$, the weight of field-free states with rotational quantum number $N > 24$ is smaller than 0.01.

In Figure 11, we present the thermal weights of the rotational excitations $\langle N \rangle_T$, defined in Equation 12, at the end of the Gaussian and centrifuge pulses with peak intensities $I_G^0 = 1.203 \cdot 10^{12} \text{ W/cm}^2$ and $I_C^0 = 5.0 \cdot 10^{10} \text{ W/cm}^2$, respectively. Note that at these intensities and for the initial states $(0, N, M_N)$, no population is transferred to the continuum. For both pulses, these thermal distributions are very similar. They show an increasing trend till reach a maximum for $N = 54$ and 42 for the GP and CP, respectively. This demonstrates the creation of samples in highly excited rotational states such as super-rotors. As the temperature increases, these maxima are reduced due to the larger weights of higher rotational excitations to the thermal sample, for which the impact of the external fields is smaller.

4 Conclusions

We have explored the ro-vibrational dynamics of Rb_2 molecules in the $a^3\Sigma^+$ electronic state, due to non-resonant light. For the

laser field, we have considered two different time envelopes having the same spectral bandwidth and carrying the same amount of energy, but inducing different dynamics. For experimentally feasible laser intensities, we find a strong coupling between the vibrational and rotational degrees of freedom. Despite the breakdown of the rigid-rotor approximation, these laser fields create wavepackets characterized by very high angular momenta. We find that the creation of these highly excited rotational excitations can result in the dissociation of the molecule even when initially in deeply bound states, in line with an earlier prediction¹⁰.

For both pulses, the lack of selection rules in the vibrational quantum number hinders the control over the vibrational bands being populated. As a consequence, the field-dressed dynamics involve states from lower and upper lying vibrational bands, with similar weights. However, a comparison of the dynamics for both pulses shows that the centrifuge one enables a better control over the vibrational excitations creating narrower distribution in this degree of freedom. Thus, the centrifuge field provokes the excitation of high rotational states while maintaining relatively low spread along the vibrational bands. This partial control over the vibrational excitations is due to the gradual transfer of energy from the centrifuge pulse to the molecule. Initially, when the centrifuge intensity is increased till the first maximum, a few neighboring vibrational bands get weakly populated, but this vibrational-rotational coupling is not significantly enhanced in the consecutive maxima. As a consequence, the centrifuge field is more efficient in creating super-rotor wavepackets with low impact on the vibrational motion. In contrast, the shorter duration of the Gaussian pulse implies that the energy is transferred faster to the molecule, and results in a stronger coupling between the vibrational and rotational motions. Thus, the amount of population that is accumulated in higher rotational excitations might be reduced, due to the larger role played by neighboring vibrational bands in the field-dressed dynamics.

The results of our work offer new perspectives on the utility of the optical centrifuge to control not only rotational, but also vibrational molecular dynamics. Our results provide guidance in, and we hope will advance, those ultrafast spectroscopic studies in which separating the rotational and vibrational excitations by intense laser pulses is of importance.

A Rigid-Rotor approximation

Within the rigid-rotor approximation, Hamiltonian of a diatomic molecule in a non-resonant laser pulse linearly polarized along the LFF Z-axis, is given by

$$H^R(t) = \frac{N^2}{2\mu} \langle R^{-2} \rangle_v + H_I^R(t) \quad (6)$$

where the first stands for the rotational kinetic energies, with the rotational constant given by $B_v = \frac{\hbar^2 \langle R^{-2} \rangle_v}{2\mu}$. The interaction of the non-resonant light with the polarizability reads

$$H_I^R(t) = -\frac{I(t)}{2c\epsilon_0} \left(\langle \Delta\alpha(R) \rangle_v \cos^2 \theta + \langle \alpha_{\perp}(R) \rangle_v \right). \quad (7)$$

The matrix elements $\langle f(R) \rangle_v = \langle \phi_{v,0} | f(R) | \phi_{v,0} \rangle_v$, with $f(R) = R^{-2}, \Delta\alpha(R)$ and $\alpha_{\perp}(R)$, and $\phi_{v,0} = \phi_{v,0}(R)$ the field-free vi-



brational wave function, adapt this approximation to the different vibrational bands of the molecular spectrum³¹. The time-dependent Schrödinger equation associated with Hamiltonian Equation 6 is solved by the short iterative Lanczos algorithm for the time propagation²¹ and a basis set expansion in terms of the spherical Harmonics for the angular coordinates³².

B Weights and matrix elements

The field-dressed dynamics is analyzed by projecting the wave packet onto the basis formed by the field-free eigenstates of the electronic state $a^3\Sigma^+$ of Rb_2 as in Equation 3. For a given initial state (v_0, N_0, M_{N_0}) , the weight of the eigenstate (v, N, M_{N_0}) to the field-dressed wave function is $|C_{v_0, N_0, M_{N_0}}(v, N, t)|^2$. To illustrate the breakdown of the rigid-rotor approximation, we calculate the population transferred to a certain vibrational band v as

$$\mathcal{V}_{v_0, N_0, M_{N_0}}(v, t) = \sum_{N=0}^{N_{\max}} |C_{v_0, N_0, M_{N_0}}(v, N, t)|^2 \quad (8)$$

where N_{\max} is the maximum number of rotational states included in the basis set expansion (3). Analogously, an accumulative rotational distribution, independent of the vibrational excitations, can be defined as

$$\mathcal{N}_{v_0, N_0, M_{N_0}}(N, t) = \sum_v |C_{v_0, N_0, M_{N_0}}(v, N, t)|^2 \quad (9)$$

where the sum runs over all vibrational bands of the Rb_2 $a^3\Sigma^+$ electronic state. At the of the pulses, we compute the mean value of the rotational excitations defined as

$$\langle \mathcal{N}_{v_0, N_0, M_{N_0}} \rangle = \frac{\sum_{N=0}^{N_{\max}} N \mathcal{N}_{v_0, N_0, M_{N_0}}(N, t_f)}{\sum_{N=0}^{N_{\max}} \mathcal{N}_{v_0, N_0, M_{N_0}}(N, t_f)} \quad (10)$$

with $t_f = t_G$ and t_C for the GP and CP, respectively. These expressions 8, 9 and 10 take into account that M_{N_0} is a good quantum number due to the azimuthal symmetry.

Due to the strong field impact, part of the population is transferred to scattering states, i.e., to the continuum. This effect is quantified by

$$P_{v_0, N_0, M_{N_0}}^D = 1 - \sum_{v, N} |C_{v_0, N_0, M_{N_0}}(v, N, t_f)|^2 \quad (11)$$

at the end of the G and C pulses, i.e., $t_f = t_G$ and t_C , respectively. The sum in Equation 11 runs over all vibrational bands, and all rotational excitations included in the numerical treatment.

For a molecular sample at temperature T , the thermal average of the rotational excitations reads as

$$\langle \mathcal{N} \rangle_T = \sum_{v_0, N_0} P_{v_0, N_0, M_{N_0}}(N, t_f) W_{v_0, N_0, M_{N_0}}, \quad (12)$$

with $t_f = t_G$ and t_C for the GP and CP, respectively. The Maxwell-Boltzmann weights are

$$W_{v_0, N_0, M_{N_0}} = \frac{g_{|M_{N_0}|} e^{\frac{E_{0,0} - E_{v_0, N_0}}{T k_B}}}{Z}, \quad (13)$$

where k_B is the Boltzmann constant, $E_{0,0}$ and E_{v_0, N_0} are the field-

free energies of the $(0, 0, 0)$ and (v_0, N_0, M_{N_0}) states, respectively. The factor $g_{M_{N_0}}$ takes into account that the impact of the laser field on the states $(v_0, N_0, |M_{N_0}|)$ and $(v_0, N_0, -|M_{N_0}|)$ is identical, so that $g_0 = 1$ and $g_{|M_{N_0}|} = 2$ for $|M_{N_0}| \neq 0$. The normalization constant is given by

$$Z = \sum_{N_0=0}^{N_T} (2N_0 + 1) e^{\frac{E_{0,0} - E_{v_0, N_0}}{T k_B}}, \quad (14)$$

where $(2N_0 + 1)$ is the field-free degeneracy in the magnetic quantum number. The highest rotational excitation included is $N_T \leq 24$. For the considered temperatures, we neglect the contribution of states in excited vibrational bands, restricting $v_0 = 0$ in Equation 13 and Equation 14. Indeed, the thermal weight for the state $(1, 0, 0)$, i.e., the rotational ground state of the first excited vibrational band, is $W_{1,0,0} = 5.9 \cdot 10^{-18}$ and $1.5 \cdot 10^{-6}$, for $T = 0.5$ K and $T = 2$ K, respectively.

To better understand the mechanism behind the population transferred to other vibrational bands, Figure 12 shows the radial matrix elements

$$\langle v, 0 | \Delta \alpha(R) | v', 2 \rangle = \int \phi_{v,0}^*(R) \Delta \alpha(R) \phi_{v',2}(R) R^2 dR, \quad (15)$$

for the non-diagonal terms in the angular operator $\cos^2 \theta$, i.e., $\Delta N = \pm 2$.

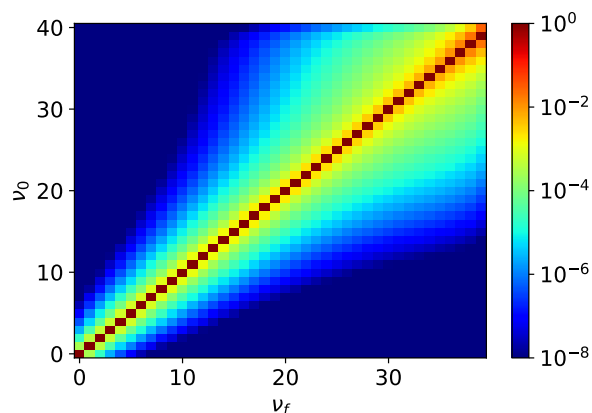


Fig. 12 Matrix elements of the vibrational part of the interaction Equation 15 between the states $(v_0, 0, 0)$ and $(v_f, 2, 0)$.

Acknowledgements

Financial support by the Spanish projects PID2023-147039NB-I00 (MICIN), the Andalusian research group FQM-207 and the Deutsche Forschungsgemeinschaft through the joint ANR-DFG CoRoMo Projects No. 505622963 (KO 2301/15-1). J.M.G.G. also acknowledges financial support by the grant PRE2021-099603 funded by MICIU/AEI/10.13039/501100011033 and by “ESF+”.

Notes and references

- 1 H. Stapelfeldt and T. Seideman, *Rev. Mod. Phys.*, 2003, **75**, 543–557.
- 2 Y. Ohshima and H. Hasegawa, *Int. Rev. Phys. Chem.*, 2010, **29**, 619–663.



- 3 S. Fleischer, Y. Khodorkovsky, E. Gershonabel, Y. Prior and I. S. Averbukh, *Isr. J. Chem.*, 2012, **52**, 414–437.
- 4 C. P. Koch, M. Lemesko and D. Sugny, *Rev. Mod. Phys.*, 2019, **91**, 035005.
- 5 J. Karczmarek, J. Wright, P. Corkum and M. Ivanov, *Phys. Rev. Lett.*, 1999, **82**, 3420–3423.
- 6 D. M. Villeneuve, S. A. Aseyev, P. Dietrich, M. Spanner, M. Y. Ivanov and P. B. Corkum, *Phys. Rev. Lett.*, 2000, **85**, 542–545.
- 7 I. MacPhail-Bartley, W. W. Wasserman, A. A. Milner and V. Milner, *Rev. Sci. Instrum.*, 2020, **91**, 045122.
- 8 A. S. Mullin, *Annu. Rev. Phys. Chem.*, 2025, **76**, 357–377.
- 9 J. Li, J. T. Bahns and W. C. Stwalley, *J. Chem. Phys.*, 2000, **112**, 6255–6261.
- 10 M. Spanner and M. Y. Ivanov, *J. Chem. Phys.*, 2001, **114**, 3456–3464.
- 11 C. Chandre and J. P. Salas, *Phys. Rev. A*, 2023, **107**, 063105.
- 12 M. Lemesko and B. Friedrich, *Phys. Rev. Lett.*, 2009, **103**, 053003.
- 13 R. González-Férez and C. P. Koch, *Phys. Rev. A*, 2012, **86**, 063420.
- 14 T. Y. Chen, S. A. Steinmetz, B. D. Patterson, A. W. Jasper and C. J. Kliewer, *Nat. Commun.*, 2023, **14**, 3227.
- 15 A. Korobenko, A. A. Milner and V. Milner, *Phys. Rev. Lett.*, 2014, **112**, 113004.
- 16 F. Lang, K. Winkler, C. Strauss, R. Grimm and J. H. Denschlag, *Phys. Rev. Lett.*, 2008, **101**, 133005.
- 17 M. Deiß, B. Drews, B. Deissler and J. Hecker Denschlag, *Phys. Rev. Lett.*, 2014, **113**, 233004.
- 18 J. Wolf, M. Deiß and J. Hecker Denschlag, *Phys. Rev. Lett.*, 2019, **123**, 253401.
- 19 X. He, K. Wang, J. Zhuang, P. Xu, X. Gao, R. Guo, C. Sheng, M. Liu, J. Wang, J. Li, G. V. Shlyapnikov and M. Zhan, *Science*, 2020, **370**, 331–335.
- 20 R. Kosloff, *J. Phys. Chem.*, 1988, **92**, 2087–2100.
- 21 M. Beck, A. Jäckle, G. Worth and H.-D. Meyer, *Phys. Rep.*, 2000, **324**, 1–105.
- 22 J. C. Light and T. Carrington, *Adv. Chem. Phys.*, 2007, **114**, 263–310.
- 23 R. Kosloff, *Annu. Rev. Phys. Chem.*, 1994, **45**, 145–178.
- 24 A. A. Milner, A. Korobenko and V. Milner, *Phys. Rev. A*, 2016, **93**, 053408.
- 25 M. Lemesko and B. Friedrich, *Phys. Rev. Lett.*, 2009, **103**, 053003.
- 26 S. Ospelkaus, K.-K. Ni, G. Quémener, B. Neyenhuis, D. Wang, M. H. G. de Miranda, J. L. Bohn, J. Ye and D. S. Jin, *Phys. Rev. Lett.*, 2010, **104**, 030402.
- 27 P. K. Molony, P. D. Gregory, Z. Ji, B. Lu, M. P. Köppinger, C. R. Le Sueur, C. L. Blackley, J. M. Hutson and S. L. Cornish, *Phys. Rev. Lett.*, 2014, **113**, 255301.
- 28 L. Holmegaard, J. H. Nielsen, I. Nevo, H. Stapelfeldt, F. Filsinger, J. Küpper and G. Meijer, *Phys. Rev. Lett.*, 2009, **102**, 023001.
- 29 I. Nevo, L. Holmegaard, J. H. Nielsen, J. L. Hansen, H. Stapelfeldt, F. Filsinger, G. Meijer and J. Küpper, *Phys. Chem. Chem. Phys.*, 2009, **11**, 9912–9918.
- 30 J. S. Kienitz, S. Trippel, T. Mullins, K. Dlugolecki, R. González-Férez and J. Küpper, *ChemPhysChem*, 2016, **17**, 3740–3746.
- 31 R. González-Férez and P. Schmelcher, *Phys. Rev. A*, 2004, **69**, 023402.
- 32 J. J. Omiste and R. González-Férez, *Phys. Rev. A*, 2013, **88**, 033416.



R González-Férez, PhD
Universidad de Granada
18071 Granada, Spain

View Article Online
DOI: 10.1039/D5CP02931G

Prof. Anouk Rijs
Editorial Office
Physical Chemistry Chemical Physics (PCCP)

July 31, 2025

Data Availability Statement

Dear Prof. Anouk Rijs,

If the manuscript "Rotational excitation of molecules in the regime of strong ro-vibrational coupling: Comparison between an optical centrifuge and a transform-limited pulse" by J.M. García-Garrido, V. Milner, C.P. Koch and R. González-Férez is accepted Physical Chemistry Chemical Physics (PCCP), we will make available the research data associated with it.

Sincerely,

Rosario González-Férez,
On behalf of all authors

